DEVELOPMENT OF TURBULENCE STATISTICS IN THE NEAR FIELD BEHIND MULTI-SCALE GRIDS

P.-Å. Krogstad

Dept. Energy and Process Eng., Norwegian University of Science and Technology, Norway

Abstract

The flows immediately behind two multi-scale grids have been studied experimentally and the results compared to data obtained behind a conventional grid. The data sets consist of measurements by means of Laser Doppler anemometry, as well as hot wire measurements using various purpose made probes. By comparing the initial turbulent energy development, as well as third and fourth order statistics, it is shown that the particulars of the grid geometry is lost after just a few mesh lengths downstream. This was further confirmed by inspecting the probability density and spectral energy distributions. Hence the present measurements suggest that the grid geometry is only important in setting the initial conditions for the turbulence development and does not affect the distributions in the far field.

1 Introduction

It has been suggested (e.g. Hurst & Vassilicos, 2007) that the flow behind multi-fractal shaped grids may have non-classical behaviour in the sense that the energy decay and mixing properties are very different from conventional grids. It was shown by Krogstad (2012) and Krogstad & Davidson (2012) that these claims are likely to be caused by most multi-fractal measurements having been performed too close to the grids and that if the measurements were extended further, conventional decay would be observed. This was based on a comparison between measurements behind two multi-scale grids that were quite similar to the Hurst & Vassilicos (2007) so-called fractal cross grids, and the results obtained from a similar size conventional grid. In order to ensure that the comparison between the data from the three grids is meaningful, the dimensions of the grids were chosen such that the integral scale of the turbulence some short distance downstream of each grid, ℓ_0, is virtually the same in all three cases (to within a percent or so). The reason for matching the integral length scales rather than some scales derived from the grid geometry is because a multi-scale grid does not have the same well defined parameters to define the geometrical parameters that affect the flow as a conventional grid. By matching the integral scales the scale is derived from the flow and therefore includes the geometrical effects on the flow. This appears to have been a good choice since the decay of turbulent kinetic energy collapses downstream of the initial wake/jet interaction region both when the data is inspected in physical space as well as when the flow is scaled with the integral length scale.

2 The experiment

The experiments were performed in the large recirculating wind tunnel described in Krogstad & Davidson (2011). The tunnel test-section has transverse dimensions of 2.7m x 1.8m (measured at the start of the test section) and is almost 12m long.

The investigation was divided into two parts. The first probed the flow development from the grid to about 25 mesh lengths downstream. In this region there are large spanwise variations and the flow develops quickly downstream. At the position where the flow uniformity was sufficiently good to assume that a power law type decay could be found, the Reynolds stresses deviated notably from isotropy, with spanwise stresses of the order of 80% of $\langle u_x^2 \rangle$.

To improve isotropy, the grid was therefore moved into the wind tunnel contraction for the far field investigation. From the location of the grid to the entrance of the test section, the area contraction ratio was 1.48 and the test section starts $x = 1.2m$ downstream of the grid. This produced a flow in the test section that starts from almost exact isotropy. (See Krogstad & Davidson, 2011, for details.) In this way the flow development has been mapped virtually from the rear face of the grid down to about 250 times the integral length scale.

All three grids were produced from $2mm$ thick sheet metal. The conventional grid has square holes $30mm \times 30mm$ punched with a spacing of $40mm$, giving a mesh size of $M = 40mm$, a bar width of $t = 10mm$, and a solidity of $\sigma = 1$ - hole area / total area = 44%. The tests on this grid were all performed at a Reynolds number of $Re_M = U_0 M/\nu = 3.6 \times 10^4$, where $U_0 = 13.5m/s$ was the mean speed in the tunnel.

The first of the multi-scale grids is shown in figure 1(a). It has bar widths ranging from $t_1 = 8mm$ down to $t_3 = 2mm$, and mesh sizes ranging from $M_1 = 64mm$ to $M_3 = 15mm$. The solidity of this mesh is also $\sigma = 44\%$. The measurements for this grid were taken at $U_0 = 14.0m/s$ which gives $Re_M = 6.0 \times 10^4$, based on M_1. The second multi-scale grid is shown in Figure 1(b). As for the first, the bar widths vary from $t_1 = 8mm$ down to $t_3 = 2mm$, though the mesh sizes are larger, with $M_1 = 88mm$ to $M_3 = 21mm$. This reduces the solidity of the second grid to $\sigma = 33\%$. This grid was tested at $U_0 = 15.5m/s$ corresponding to $Re_M = 9.1 \times 10^4$.

The turbulence produced by these grids becomes homogeneous and fully developed well upstream of $x = 2m$, at which point the turbulence is uniform across the grid to within $\pm 0.5\%$. The Kolmogorov microscale ranges from $\eta \approx 0.22$mm to 0.26mm here. At this position the grids were designed to have the same integral scales which were measured to be $\ell_0 = 23.9mm$ (for the conventional grid), $\ell_0 = 23.6mm$ (for the first multi-scale grid), and
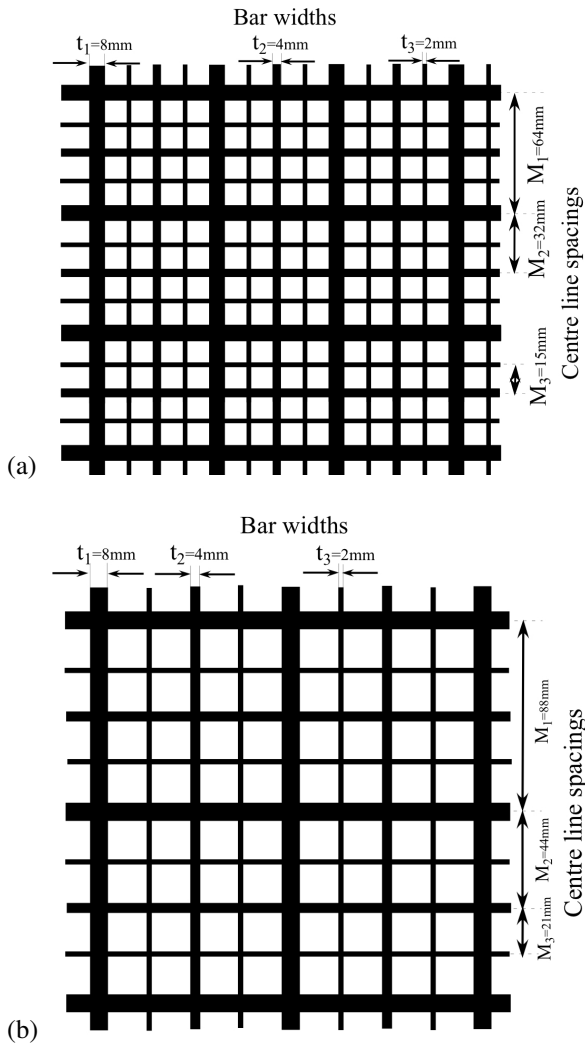
Figure 1. The two multi-scale grids used. a) High solidity grid, b) low solidity.

$\ell_0 = 23.4mm$ (for the second), respectively. Note that the geometric length-scales associated with the two multi-scale grids almost span the full range of dynamical scales associated with the turbulence, from around 9η up to several integral scales. Finally it may be noted that, in terms of ℓ_0, the tunnel cross-section is approximately $115\ell_0 \times 80\ell_0$, thus ensuring that there was minimal influence from the side-wall boundary layers on the measurements, which were taken along the tunnel centre line.

The data for the near field was obtained using single component hot-wire anemometry, as well as two-component laser Doppler anemometry. The hot-wire measurements were done using a purpose made $2.5\mu m$ partly etched Platinum-10%Rhodium straight single wire. The active wire length was $0.5mm$.

In the near field, occasional reversed flows are encountered behind the bars and thus very high turbulence levels may be expected. In this situation hot wire anemometry is not a suitable measurement technique. Therefore two component laser Doppler anemometry (LDA) was primarily used to map the near grid turbulence field. A Dantec fiber optical probe with a focal length of $300mm$ was used together with a $400mW$ air cooled Spectra Physics laser, and the signal was processed using a Dantec burst analyzer. This system has a probe volume which is 2.3 and $2.2mm$

long with a diameter of 0.15 and $0.14mm$ in the streamwise and spanwise directions respectively. 100.000 samples were taken in coincidence mode for each point and the data was corrected for velocity bias using transit time weighting.

3 Results
3.1 Statistical moments

In Krogstad & Davidson (2012) the development of the spanwise non-homogeneity downstream of the grid is documented and it is shown that for all grids the spanwise variation in the turbulence statistics is negligible from $x \approx 1200mm$ from the grid, which corresponds to $x/M_1 \approx$ 30, 19 and 14 for the conventional, multi-scale 1 and multi-scale 2 grids, respectively. (M_1 is the size of the largest square formed by the grid, see figure 1.)

Upstream of this point the flow development is dependent on the path followed. This is demonstrated in figure 2(a), which shows the development along two separate lines for each grid. (The data has been normalized with the bulk velocity, U_0, and the grid pressure drop coefficient, C_P.) The data labelled "hole" develops along a line that starts from the centre of a hole in the grid. Similarly, the data labelled "cross" starts from the intersection of the largest bars forming the grid. After about $x/M_1 \sim 10$ to 20 the data for all lines collapse and start to decay at about the same rate. This determines the end of the near field and the start of the homogeneous decay.

This decay is shown in figure 2(b). For the conventional and first multi-scale grid the turbulence decays at virtually identical rates all the way down to the end of the range investigated ($x/M_1 \approx 240$ for the conventional grid). The decay exponent was found by Krogstad & Davidson (2011) to be $n \approx$ -1.13 for the conventional grid and $n \approx$ -1.12 for multi-scale grid 1, respectively. For the second multi-scale grid, the data sits consistently lower than for the other two grids and the decay rate was slightly faster with $n \approx$ -1.25. These exponents are very close to the values obtained for most investigations of grid turbulence, e.g. from the cryogenic experiment of White et al. (2002) values of n between 1.15 and 1.22 were reported. Lavoie et al. (2007) looked at the effect of grid bar shapes and suggested values of n from 1.05 to 1.24.

During this early development, the flow is far from being Gaussian, as shown by the developments of the velocity skewness- ($S_p =< p^3 > / < p^2 >^{3/2}$) and flatness-factors ($F_p =< p^4 > / < p^2 >^2$) (see figure 3). However, all flows quickly tend towards a state which is close to, but not quite Gaussian, with $S \to 0$ and $F \to 3$. The measurements reported in Krogstad & Davidson (2011) showed that this state is never reached even at the end of the far field. S_u was always slightly positive, which it needs to be in a spatially decaying flow, while F_u remained constant at $F_u \approx$ 2.95. Figure 3 shows that the trend for the two multi-scale grids are the same when the streamwise distance is scaled with M_1 and within two to three mesh lengths the flow has reached a state where S and F are independent of the streamwise position. For the conventional grid the distance needed is somewhat longer with the asymptotic values reached for $x/M_1 \gtrsim 10$. That the conventional grid needs more time to reach some sort of equilibrium is not unexpected, since the multi-scale grids contain many more bars that enhances the initial mixing.

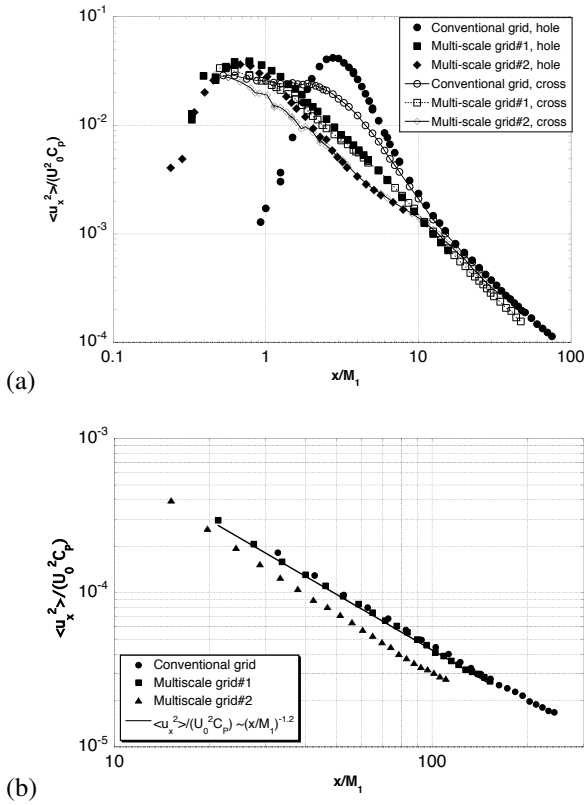The development of the second, third and fourth order moments of the streamwise fluctuations ($< u_x^2 >$, skew-

(a)

(b)

Figure 2. The development of $< u_x^2 >$ as function of distance from the grid. a) Near the grid, b) in the homogeneous region.
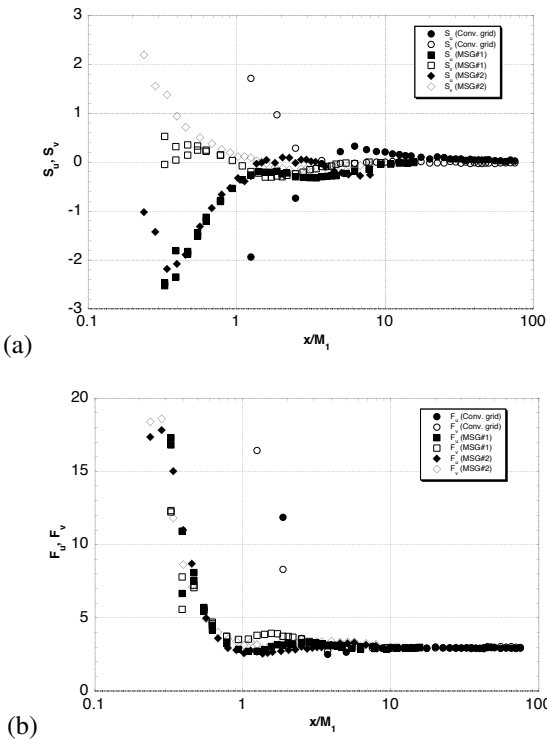

(a)

(b)

Figure 3. Skewness and flatness distributions along a line starting from the centre of a hole. a) S_u and S_v, b) F_u and F_v. Filled symbols are for u and open symbols for v.
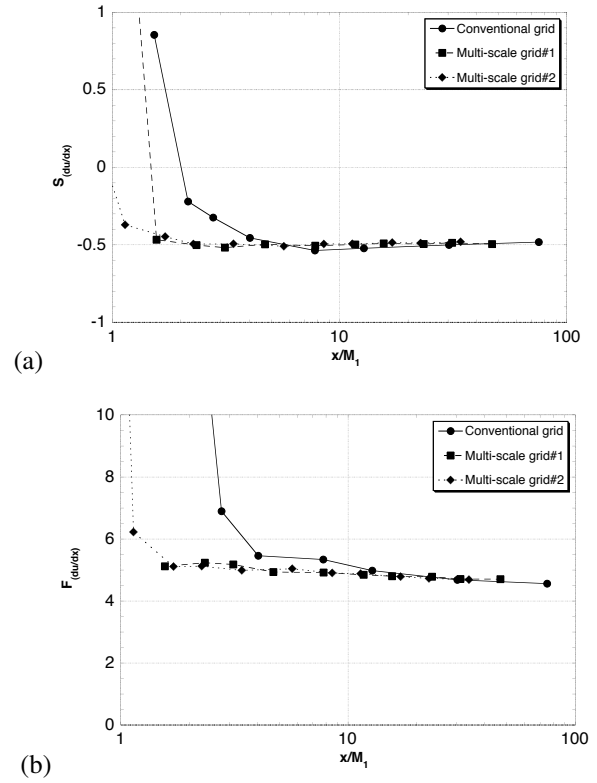

(a)

(b)

Figure 4. Skewness and flatness of streamwise velocity derivatives measured along a line starting from the centre of a hole. a) $S_{\partial u/\partial x}$, b) $F_{\partial u/\partial x}$.

ness and flatness factors) all indicate that after a rather short initial grid-dependent flow development, the statistics of the energy carrying structures are indistinguishable. In order to check if the same applies to the small scale motion which controls the dissipation rates, the skewness and flatness of the streamwise velocity derivatives $(S_{\partial p/\partial x} =< (\partial p/\partial x)^3 > / < (\partial p/\partial x)^2 >^{3/2}$ and $F_{\partial p/\partial x} =< (\partial p/\partial x)^4 > / < (\partial p/\partial x)^2 >^2)$ are shown in figure 4. $S_{\partial p/\partial x} =< (\partial p/\partial x)^3 > / < (\partial p/\partial x)^2 >^{3/2}$ is a measure of the small scale stretching mechanism and was shown by Burratini et al. (2008) to be constant in the homogeneous decay region at -0.5 ±5%. This agrees well with the data of Frenkiel & Klebanboff (1971) and the present data shown in figure 4(a). The flatness of the streamwise derivative of u_x shown in figure 4(b) is related to the small scale intermittency (see e.g. Frenkiel & Klebanboff, 1971), and needs to be higher than 3 if the statistics of the turbulent motion is otherwise Gaussian. Figure 4 confirms that also the small scale motion appear to be independent of the grid geometry except for a very short initial development region which is only a few mesh lengths long.

3.2 Probability density functions

Hence it is expected that the probability density functions of the turbulent motion must also collapse after a short distance from the grid. In figure 5 the probability density functions of u, measured at $x/M_1 = 1.25$ and 12.5, respectively, are shown. At the first station (left figure) the pdfs for the two multi-scale grids are almost identical and rather close to being Gaussian, whereas the pdf for the conventional grid is slightly skewed near the centre and contains large positive and negative excursions, consistent with the
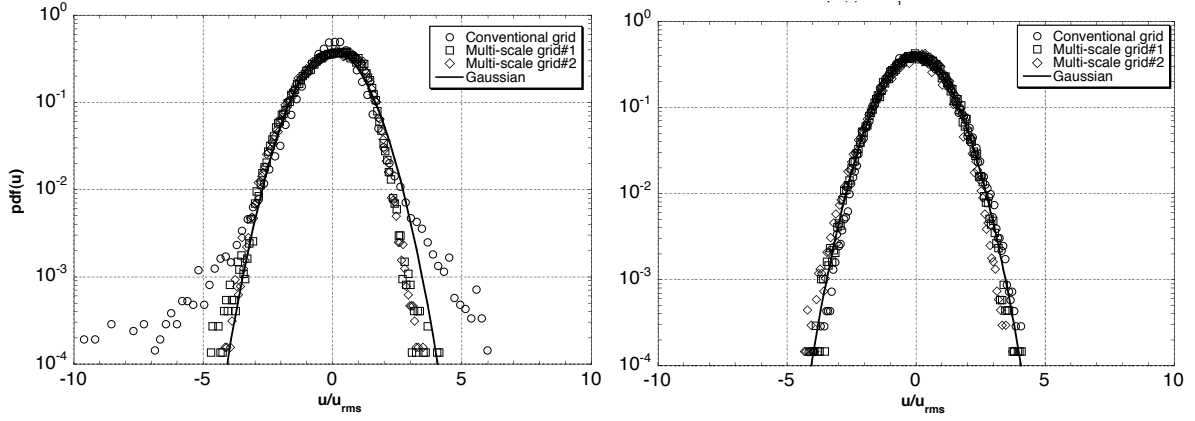
3

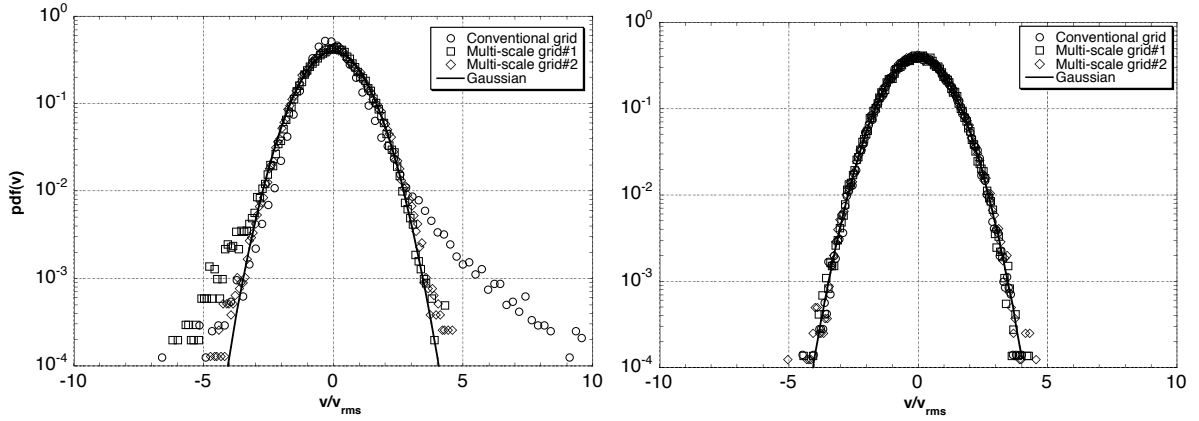Figure 5. $pdf(u)$ measured at x/M_1=1.25 (left) and 12.5 (right).

Figure 6. $pdf(v)$ measured at x/M_1=1.25 (left) and 12.5 (right).
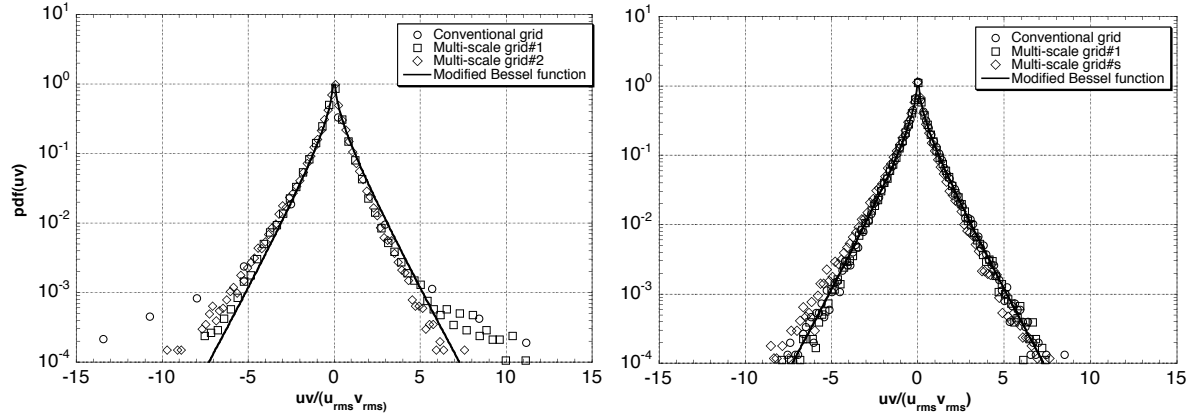

Figure 7. $pdf(uv)$ measured at x/M_1=1.25 (left) and 12.5 (right).

high flatness factors observed in figure 3. Similarly, figure 6 demonstrates the same behaviour for the v component.

After about ten mesh lengths the characteristics of u and v are Gaussian, following the distributions

$$pdf(u) = \frac{e^{\left(-\frac{u^2}{2u_{rms}^2}\right)}}{u_{rms}\sqrt{2\pi}}, \quad pdf(v) = \frac{e^{\left(-\frac{v^2}{2v_{rms}^2}\right)}}{v_{rms}\sqrt{2\pi}}. \quad (1)$$

The probability density of the product of the two velocity components is then given by the expression

$$pdf_{uv}(z) = \int_{-\infty}^{\infty}\int_{-\infty}^{\infty} \frac{e^{\left(-\frac{u^2}{2u_{rms}^2}\right)}}{u_{rms}\sqrt{2\pi}} \frac{e^{\left(-\frac{v^2}{2v_{rms}^2}\right)}}{v_{rms}\sqrt{2\pi}} \delta(uv-z)\,dudv$$

$$= \frac{K_0\left(\frac{|\ell|}{u_{rms}v_{rms}}\right)}{\pi}, \quad (2)$$

where K_0 is the modified Bessel function of the second kind. Figure 7 shows the probability distributions for the shear stresses at the same stations. For small to moderate stresses (e.g. $|uv|<5$), the model for the two Gaussian products represents the distributions for all grids very well at all stations. This suggests that the small scale motion is close to Gaussian almost immediately after the flow leaves the grid. Further downstream ($x/M_1 = 12.5$) the small number of events that exhibit strong correlations quickly disappear due to the intense interaction with other structures, leaving

the flow virtually Gaussian in all respects.

From this we conclude that it is only the flow in the immediate vicinity of the grid that is sensitive to the grid geometry.

3.3 Power density spectra

One of the unique properties that have been claimed for multi-scale grids is that energy is injected at a high number of scales. This ought therefore generate a flow that is in equilibrium much faster, since the energy is initially spread over a large range in the spectrum. Many characteristic length scales may be extracted from a grid. The most obvious are the scales associated with the dimensions of the bars that form the grid, as well as the dimensions of the holes, i.e. t_i and M_i in figure 1.

In figure 8 a spectrum measured at $x/M_1 = 20$ behind multi-scale grid 1 is shown together with arrows showing the non-dimensional wave numbers derived from the grid. It is obvious that in this experiment the geometric scales are distributed almost over the entire range of turbulent energy containing scales present in the flow. The spectrum shows that the energy injected at these scales have long since been smeared out over neighboring scales, so that the spectrum appears completely smooth. A similar distribution is found for the other multi-scale grid. Hence the suggestion of rapid initial mixing appears to be justified.

For the conventional grid, however, there are only two scales, one when using the mesh size, M, which is located at $k\eta = 2\pi\eta/M \approx 0.015$ at this x/M position, and one at $k\eta \approx 0.060$ when using t, i.e. near the upper and lower ends of the Kolmogorov inertial region. This produces more distinct vortex shedding footprints, and so the energy input around these scales appear to live much longer. We demonstrate this by showing a comparison between spectra obtained for the three grids at $x/M_1 \approx 2.3$.
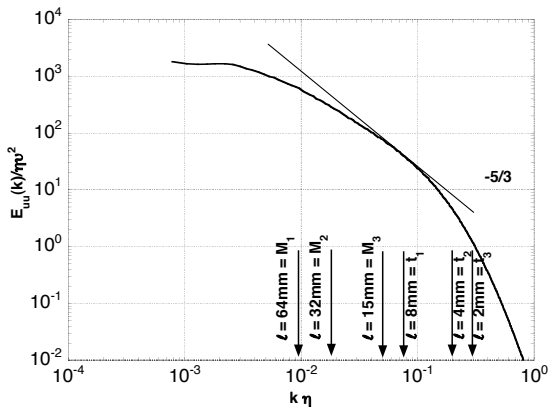

Figure 8. Kolmogorov scaled one-dimensional u_x-spectrum obtained for multi-scale grid 1 at $x/M_1 = 20$. The arrows indicate the scales derived from the grid geometry.

The spectra (figure 9(a)) show that the energy distribution for the two multi-scale grids has been distributed evenly over all scales even as close to the grid as $x/M_1 \approx 2.3$ and the two spectra collapse over most of the wave numbers. Only at very large scales ($k\eta < 0.001$) is there a small difference because the flow behind the grid with the lowest solidity needs slightly more time to reach equilibrium at the largest scales.
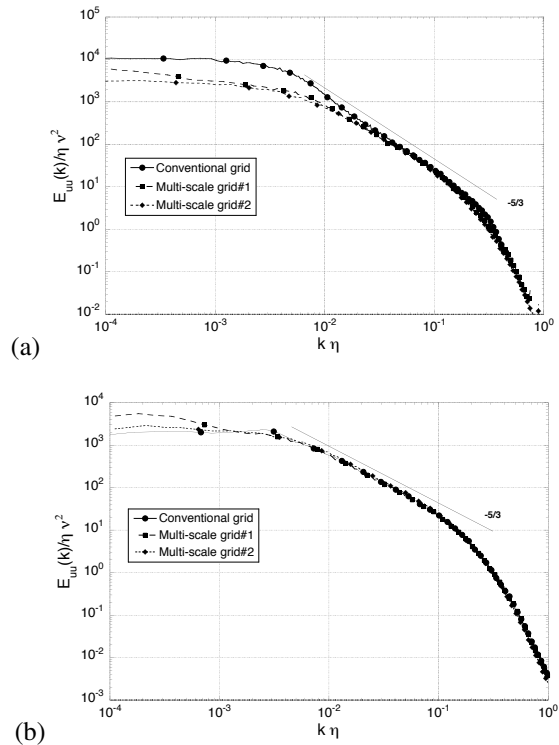

(a)

(b)

Figure 9. One-dimensional u_x-spectra for the three grids measured at a) $x/M_1 \approx 2.3$ and b) $x/M_1 \approx 12$.

In the spectrum for the conventional grid there is distinct evidence of energy input in the form of a bulge at the expected wave number of around $k\eta \approx 0.007$, and another near $k\eta \approx 0.25$. The first corresponds to the wave number given by the mesh size ($k\eta = 0.0072$). The origin of the second bump is less clear, as it represents a length scale of about $1mm$, which is only about one tenth of the bar width. However, as the flow moves downstream, these bumps quickly disappear and at $x/M_1 \approx 12$ (figure 9(b)) the spectra collapse completely over all wave numbers except for the very largest scales, where the spectra are less reliable.

In order to investigate more closely how the near grid differences die out, the power density spectra were computed for all measurement stations taken in the near field. By combining the pre-multiplied spectra to generate a contour map, the spectral energy development in the near field may be visualized. In figure 10 we have plotted $\log\left[kE_{uu}(k)/U_{ref}^2\right]$ as function of the wave number normalized by the largest grid dimension, kM_1, and the normalized distance from the grid, x/M_1. It may now be seen that while the energy is concentrated over a rather limited range of scales as the flow leaves the conventional grid (figure 10(a)), it is spread over a much wider range of scales for the multi-scale grid. This is of course to be expected since the purpose of the grid was to generate turbulent kinetic energy at a large number of scales.

As the flow moves downstream, the eddies at the various scales start to interact and the strong shear along the edges of the wake behind the bars cause significant energy production. Since the hole in the multi-scale grid is much smaller than for the conventional grid ($18mm$ compared to $30mm$), this process happens earlier for the multi-scale grid than for the conventional one, when following a line that starts from the centre of the hole. Therefore the peak in kinetic energy is reached earlier for the multi-scale grid than
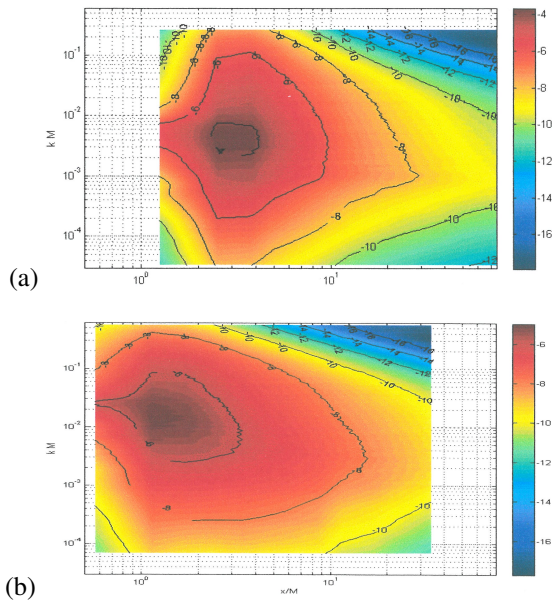
(a)

(b)

Figure 10.   Pre-multiplied energy maps for lines starting at the centre of a hole. a) Conventional grid and b) Multi-scale grid 2.

for the conventional grid, as was demonstrated in figure 2(a).

The peak in the pre-multiplied energy spectra for the conventional grid is found at $x/M_1 \approx 3$, while for the multi-scale grid it is found at $x/M_1 \approx 1.2$. However, the wave number range for the energy containing scales is much wider for the conventional grid. Whereas the maximum extent of the contour $\log\left[kE_{uu}(k)/U_{ref}^2\right]$ = -8 for the multi-scale grid at $x/M_1 \approx 1$ goes from $kM_1 \approx 2.5 \times 10^{-4}$ to about 0.4, i.e. 3 decades, the span for the conventional grid at $x/M_1 \approx 3$ is from $kM_1 \approx 3 \times 10^{-5}$ to 0.3 or about 4 decades. This suggests that it is mainly the small scale energy distribution that comes off the grid which is different.

However, from $x/M_1 \approx 10$ to 15 the spectra for the two flows are almost identical when scaled with M_1.

4   Conclusions

The initial turbulence development behind two multi-scale grids have been measured and the data compared to measurements for a conventional grid. The evolution of the kinetic energy very near the grid, exemplified by data for the streamwise normal stress, $<u_x^2>$, is shown to depend strongly on the path followed from the grid. However after only about 10 mesh lengths, the energy decay rate is the same for all grids, following $<u_x^2> \sim x^{-n}$, where n is of the order of 1.2. This is consistent with what is found in most other grid experiments (e.g. Burattini et al, 2008, and White et al, 2002). Also higher order statistics, like skewness and flatness of u_x and u_y, as well as skewness and flatness of the

velocity derivative in the streamwise direction indicate that there are no measurable differences in the flows if the initial region is excluded from the analysis.

It is also demonstrated that the probability density distributions of the streamwise and spanwise velocities collapse for all grids for $x/M_1 > 10$ and become close to Gaussian. The same good agreement is also found for the probability distributions of their products.

Finally the streamwise evolution of the spectral energy distribution is examined. It is shown that very close to the grid the range of scales is very much dependent on the grid geometry. However, after a very short distance the turbulent energy has been redistributed in such a way that the spectra collapse over four orders of scale magnitude.

The present data does not give support to the claims that grids composed of many length scales have unusual and non-classical flow characteristics. It may not be concluded from the present set of data that some grids based on fractal geometries do not exhibit very special mixing and energy decay properties, as has been suggested by e.g. Hurst & Vassilicos (2007), since our geometries do not cover all the geometries investigated by Hurst & Vassilicos. But it appears rather unlikely that some multi scale grids produce significantly differrent results in the far field based on the very rapid collapse observed in all the properties investigated for the grids used in the present study.

References

Burattini, P., Lavoie, P. & Antonia, R.A., 2008, "Velocity derivative skewness in isotropic turbulence and its measurement with hot wires", Exp. Fluids, Vol. 45, pp. 523-535

Frenkiel, F.N. & Klebanoff, P.S., 1971, "Statistical properties of velocity derivatives in a turbulent field", J. Fluid Mech, Vol. 48, pp. 183-208

Hurst, D. & Vassilicos, J.C., 2007, "Scaling and decay of fractal-generated turbulence", Phys. Fluids, Vol. 19, 035103

Krogstad, P.-Å., 2012, "Turbulent decay in the near field of multi-scale and conventional grids", Int. J. Heat and Fluid Flow, Vol. 35, pp. 102-108

Krogstad, P.-Å. & Davidson, P.A., 2011, "Freely decaying, homogeneous turbulence generated by multi-scale grids", J. Fluid Mech, Vol. 680, pp. 417-434

Krogstad, P.-Å. & Davidson, P.A., 2012, "Near-field investigation of turbulence produced by multi-scale grids", Phys. Fluids, Vol. 24, 035103

Lavoie, P., Djenidi, L. & Antonia, R.A., 2007, "Effects of initial conditions in decaying turbulence generated by passive grids", J. Fluid Mech, Vol. 585, pp. 395-420

White, C.M., Karpetis, A.N. & Sreenivasan, K.R., 2002, "High-Reynolds-number turbulence in small apparatus: grid turbulence in cryogenic liquids", J. Fluid Mech, Vol. 452, pp. 189-197